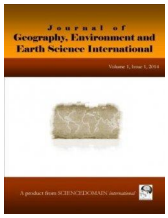

Journal of Geography, Environment and Earth Science International

17(2): 1-19, 2018; Article no.JGEESI.44047
ISSN: 2454-7352

Modelling the Relationship between Urban Growth Modes and the Thermal Environment - A Case Study of the Barasat Municipality, West Bengal

Kasturi Mukherjee[1*] and Pannalal Das[1]

[1]Department of Geography, University of Calcutta, India.

Authors' contributions

This work was carried out in collaboration between both authors. Author KM designed the study, managed the literature search performed the statistical analysis and wrote the first draft of the manuscript. Author PD managed the analyses of the study. Both authors read and approved the final manuscript.

Article Information

DOI: 10.9734/JGEESI/2018/44047
Editor(s):
(1) Dr. Abida Farooqi, Assistant Professor, Department of Environmental Sciences, Quiad-i-Azam University, Pakistan.
(2) Dr. Wen-Cheng Liu, Department of Civil and Disaster Prevention Engineering, National United University, Taiwan and Taiwan Typhoon and Flood Research Institute, National United University, Taipei, Taiwan.
Reviewers:
(1) Eric S. Hall, USA.
(2) C. R. Ramakrishnaiah, Visvesvaraya Technological University, India.
(3) Ngakan Ketut Acwin Dwijendra, University of Udayana, Indonesia.
Complete Peer review History: http://www.sciencedomain.org/review-history/26489

Original Research Article

Received 04 July 2018
Accepted 15 September 2018
Published 01 October 2018

ABSTRACT

The transformation of the rural landscape through industrialisation, urbanisation and rural-urban migration contributes to the physical growth of cities using 'built-up' development, known as urban sprawl. Urban sprawls are often associated with the increase of Land Surface Temperature (LST) in both magnitude and spatial extent which modifies the urban thermal environment, attributable to a phenomenon known as the Urban Heat Island (UHI). Not all the urban growth is sprawl, and not all urban growth is necessarily detrimental to the environment. Measuring urban growth instead of sprawl, allows us to quantify the amount of land that has been converted to urban land use. In this project, three major types of urban growth, i.e. infilling, edge expansion, and leapfrog development have been identified and quantified from the built-up dynamics. Landsat Thematic Mapper (TM), Enhanced Thematic Mapper Plus (ETM+) and Operational Land Imager/Thermal Infrared Sensor (OLI/TIRS) images were used to estimate LST, and to extract the built-up area for this study. To

**Corresponding author: E-mail: jscorpio.8@gmail.com;*

understand the impact of these urban growth modes on the thermal environment, two methodologies have been adapted: i) GIS-based sectoral-buffer analysis, and, ii) Partial Least Square Regression (PLSR). They analyse and quantify the relative importance of urban growth modes in controlling the changing pattern of LST. The methods have been applied in the Barasat municipality, West Bengal, India. The study reveals that different types of urban expansions have different effects on the thermal environment. Edge expansion is the most important factor in determining LST change. This study may provide information contributing to a better understanding of urban development. Lowering the heat island effect may be possible through well-managed urban growth.

Keywords: Landscape Expansion Index (LEI); urban growth mode; infilling; edge expansion; leapfrog development; Land Surface Temperature (LST); Surface Urban Heat Island (SUHI); sectoral buffer analysis; Partial Least Square Regression (PLSR).

1. INTRODUCTION

The environmental impacts of the widespread transformation of the rural landscape through industrialisation, urbanisation, and rural-urban migration are the major concerns of the late twentieth and early twenty-first centuries [1]. As of the year 2010, 50.5% of the world's population lived in urban areas [2]. The rate of urbanisation and population growth in India is faster than expected under the Influence of its rapidly growing economy. Urban population in India has increased drastically from 62 million in 1951 to 377 million in 2011 [3] and is expected to be 600 million by 2031 [4]. This kind of population pressure, and resultant urbanisation, has contributed to the physical growth of cities using built-up development, known as urban sprawl. The process of transforming the nonurban land into urban land causes the process of, urban sprawl to facilitate the destruction of open spaces, natural vegetation, and loss of farmlands. Sprawls are often related to uncontrolled, unsuitable scattered and fragmented development, leading to intensification of the Urban Heat Island (UHI) effect and other environmental degradation [5]. Despite of all the concerns, the concept of 'sprawl' suffers from a problem of not having any universally accepted definition. Not all the urban growth is sprawl. Moreover, sprawl has a negative implication on the environment, but all urban growths are not necessarily detrimental to the environment [5]. To mitigate these effects, and for sustainable future urban planning, urban growth needs to be studied, understood, quantified and analysed at different spatial and temporal dimensions.

Measuring urban growth allows us to quantify the amount of land that has been converted to urban use. This will also help to identify different patterns of urban expansion. Three major types of urban growth modes that have been widely discussed, by assessing the location and spatial association of new urban development about the existing urban structures, are infilling, edge expansion, and leapfrog development [6,7,8]. Infilling refers to the development of new urban land in the vacant spaces of existing urban 'patches'. Infilling is surrounded by the old urban land [9]. Expansion taking place at the boundaries of already urbanised areas is termed as edge expansion or outlying expansion [10]. Scattered urban development, not directly attached to the existing built-up, is known as leapfrog expansion. Availability of low- cost land for development, away from the core IOF the vacant suburban areas, encourages builders to develop low density discontinuous urban structures. These three modes of expansion have been used to understand the spatio-temporal growth modes of urban areas in this study.

A well recognised effect of land conversion, due to unplanned urban growth, is the formation of UHIs [11]. The atmospheric 'warmth' of a city in contrast to it's adjoining rural area is called a UHI [12,13]. The urban landscape differs from rural regarding building density, structure and materials used for roadways and buildings. Dark surfaces such as asphalt used for roadways and roofs tend to have low albedo [14]. They can absorb a higher amount of solar radiation and convert it to thermal energy. As a result, surplus heat energy accumulates in the urban environment and is likely to have more heat than its suburban and rural counterparts during the daytime. This phenomenon of high temperatures in the urban core, compared to the adjoining rural areas, is referred as UHI. The older the urban

area is, the more heat can be stored by the building materials, trapped by street canyons, and emitted by human activities. Heat loss is lower because of the reduced vertical flux change [15,16].

Heat islands can be separated into three classes: boundary layer heat islands (BLHI), canopy layer heat islands (CLHI), and surface urban heat islands (SUHI). The urban canopy layers expand upwards from the surface to building height, and the urban boundary layer is situated above the canopy layer [17]. The CLHI and the BLHI are called atmospheric heat islands, and they indicate hotter urban atmospheres. The SUHI refers to the comparative higher temperature of urban surfaces as compared to the surrounding rural areas. Atmospheric UHIs become stronger at night, while surface e UHIs is happening to be stronger during the day [18]. The Surface Urban Heat Sinks (SUHS) generate a cooling effect and offer the greatest heat stress relief to a city. A SUHS arises from evaporative trees and lawns in a city [19]. Land Surface Temperature (LST) is believed to correspond strongly with the SUHI and SHUS [20]. Thermal infrared (TIR) remote sensing presents an exclusive method for collecting LST information at the regional and global scales. In this spectral region, most of the energy read by the sensor is directly emitted by the land surface [21]. The variation in LST in the warmer city core and its surroundings helps to define the SUHI and SUHS. The temperature variation within city limits is called the Intra-Urban Heat Islands (IUHI) [22].

However, problems arise when the comparison of absolute LST values obtained on different dates under different atmospheric conditions is required to quantify SUHI or SUHS from a temporal perspective [23]. Standardisation of LST facilitates comparison of LST values retrieved from different satellite images of different dates. Standardisation of the LST is the method of defining how many image pixels are below or above the mean LST value in the whole LST sample, determined from the standard deviation [24]. The areas having values higher than the zonal mean are the areas of relatively higher temperature. They are considered thermal 'hotspots'. The values lower than the zonal mean are comparatively cooler areas, known as 'cool spots'. In this way, it is possible to distinguish between the hot and cold zones which are thermally stable [24]. The SUHI is characterised by hotspots, whereas SUHS is characterised by cool spots.

The effects of urban expansion on the formation of UHIs have been previously studied and documented [25,26,27,28]. Most of the studies have shown that the SUHI phenomenon of thermal hotspots are related to urbanisation [29,30,31,32,33,34,35,36,37,38,39] while, SUHS are associated with urban greenery [40,41,42]. The quantification of growth modes has been done to understand the various aspects of urban growth like trends, direction, and speed [5,43,44]. However, there is a lack of in-depth study to understand the effects of the urban growth on the thermal environment. Very little is known on the attribution of thermal hotspots, and cool spot magnitude to different urban growth modes.

This paper attempts to provide insight into the impact of different urban growth modes on thermal environments, and two methodologies has been adapted to accomplish this. LST have been retrieved and standardised to distinguish the hotspots and cool spots. The spatio-temporal dynamics of the different urban growth modes, hotspots, and cool spots have been analysed by GIS-based sectoral-buffer analysis. The relative importance of urban growth modes on controlling the changing pattern of LSTs has been assessed using Partial Least Square Regression (PLSR).

The methodologies presented in this paper are used to assess the impacts of urban growth modes on the thermal environment. The assessment can assist policy makers and urban planners in decision making to adopt suitable measures for improving the quality of the urban environment in the developing cities, where more urban growth is still likely to occur.

The methodologies have been demonstrated in the Barasat municipality, West Bengal, India. The study aims at identifying the spatiotemporal dynamics of urban expansion between 1989 and 2017. It quantifies the different urban growth modes in three phases (i.e. 1989-2001, 2001-2014 and 2014-2017). The study attempts to analyse the impact of the urban growth modes on the modification of the thermal environment over the study period.

The next section describes the study site. Materials and methods are presented in section 3. Section 4 is dedicated to the result and discussion, which includes the presentation of: (i) the urban growth of the study area from 1989 to 2017, (ii) the sectoral distribution of different types of growth modes, hotspots and cool spots in the study area, (iii) the relative importance

urban growth modes on controlling changing pattern of LST. Section 5 concludes the analysis.

2. STUDY AREA

The North 24 Parganas District of West Bengal is the most populated district of India according to the census of 2011. It has a long history of urbanisation from colonial times because of its industrial and administrational sectors. Barasat (Fig. 1) has become a non-industrial administrative headquarter town of the North 24 Paraganas District in 1986. Since then it has become the district headquarter, and its importance has increased. Numerous important roads like the Jessore Road National Highway 34, etc. cross through this municipality. The municipality started to became populated following the creation of Bangladesh in 1971. With a 125% population growth rate between 1991 and 2011, the fast pace of population growth in Barasat has become more noticeable in recent decades. The non- urban landscape of this area is being altered continuously and being converted into urban land. The rapid, hasty urbanisation associated with the population growth has become a significant challenge in this area.

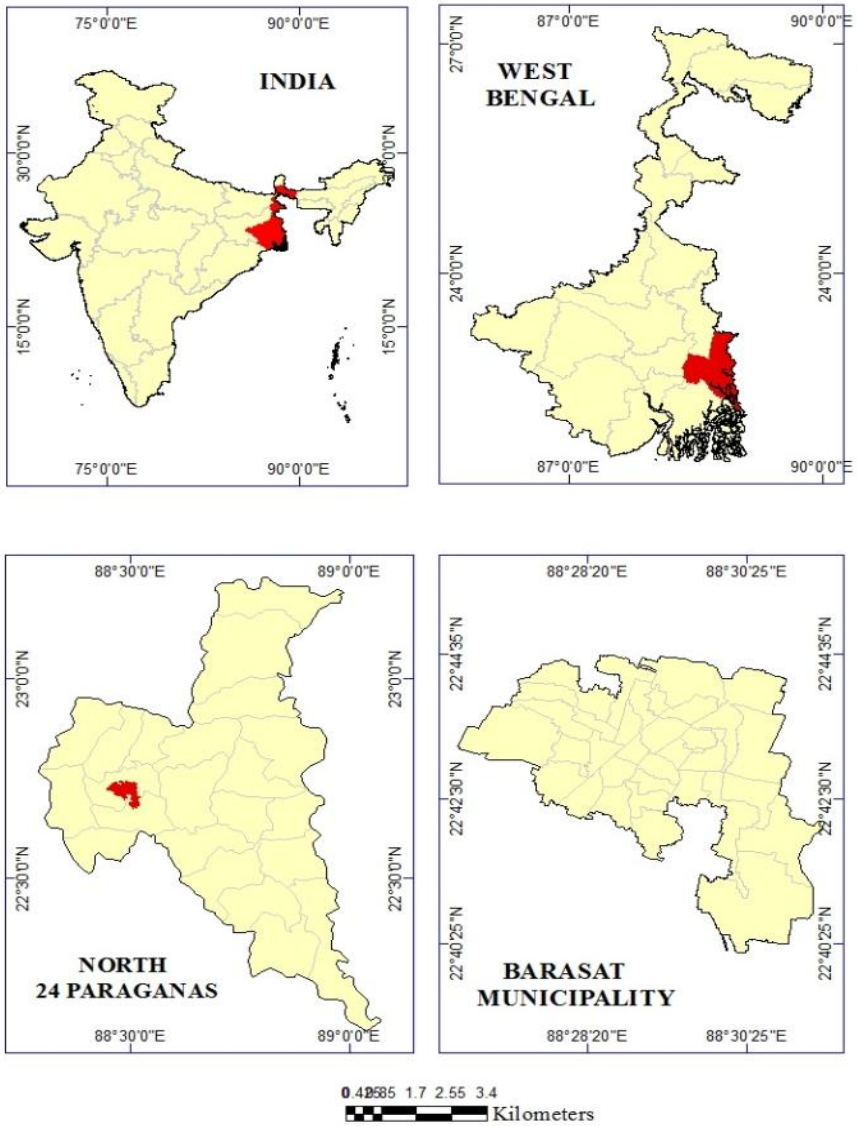

Fig. 1. Location map of the study area

3. MATERIALS AND METHODS

3.1 Data

To display the area, the satellite image tile of 138 Path and 44 Row has been downloaded free from the United States Geological Survey (USGS) website for all of the study periods. The acquired images were corrected radiometrically and geometrically. Atmospheric correction was not performed since the images were cloud free [45,46]. Based on the topographical map (sacle-1:50000), the administrative map of Barasat was registered in the Universal Transverse Mercator (UTM) (Zone 45) and World Geodetic System (WGS84). The rectified map of Barasat was used to subset the processed images. Then, the clipped images were used as inputs to generate the Land Surface Temperature, and extract the urban built-up of 1989, 2001, 2014 and 2017 (April) for this study. It is noteworthy that the image processing was performed by TNT MIPS Pro 2015, ARC GIS Desktop 10.1**,** and the XLSTAT platform. The details of the sensors used in this study have been documented in Table 1.

3.2 Built-up Area Extraction

To study the urban dynamics, the built-up area of 1989, 2001, 2014, and 2017 was required. The clipped images were classified into built-up and non-built-up [47]. The built-up category of the classified maps includes settlements, infrastructures, industrial areas, road network, pavements, and man-made structures, while the non- built-up consists of all other types of land use and land cover present in the study site. These images were classified into thematic layers of built-up and non- built-up classes using the supervised maximum likelihood classifier algorithm [48,49,50]. However, for this study binary maps were prepared from the classified land use map by using the reclassification technique of ArcGIS. The binary images have the built-up class as one, and the non-built-up class as zero. The binary images were then vectorised to get the vector files of built-up areas of Barasat for all of the years.

3.3 Identification and Quantification of Urban Growth Modes

To understand the different growth modes (infilling, edge expansion and leapfrog expansion) the entire study period has been classified into three phases, namely, 1989–2001, 2001–2014, and 2014–2017. The Landscape Expansion Index (LEI) [51] was used to identify and quantify the urban growth modes.

$$LEI = \frac{L_C}{P} \quad (1)$$

Where, L_C is the length of the shared boundary of the pre-existing urban patch and a newly grown urban patch, and p is the perimeter of this newly grown urban patch. The urban growth type is identified as infilling development when $LEI \geq 0.5$. When $0 < LEI < 0.5$, it is edge expansion, and leapfrog expansion is identified when $LEI = 0$ which indicates no common boundary. An example of different growth modes in the study area is illustrated in Fig. 2.

3.4 Land Surface Temperature Estimation

3.4.1 Calculation of land surface temperature (LST) from Landsat 5 TM and landsat 7 ETM+ Data

Single-Channel algorithm was used for LST estimation. This process includes conversion of (1) digital number (DN) to sensor spectral radiance; (2) spectral radiance to surface-escaping radiance; (3) radiance to ambient radiant temperature; and (4) ambient radiant temperature to surface temperature [52].

Table 1. Details of sensors data used

Year	1989	2001	2014	2017
Satellites	Landsat 5	Landsat 7	Landsat 8	Landsat 8
Sensors	TM	ETM	OLI/TIRS	OLI/TIRS
Date	1989-04-25	2001-04-26	2014-04-22	2017-04-14
Path/Row	138/044	138/044	138/044	138/044
Spatial Resolution	Optical-30m, Thermal-120m	Optical-30m, Thermal-120m	Optical-30m, Thermal-120m	Optical-30m, Thermal-120m
Spectral Bands	7	7	11	11
Radiometric Resolution	8	8	8	8

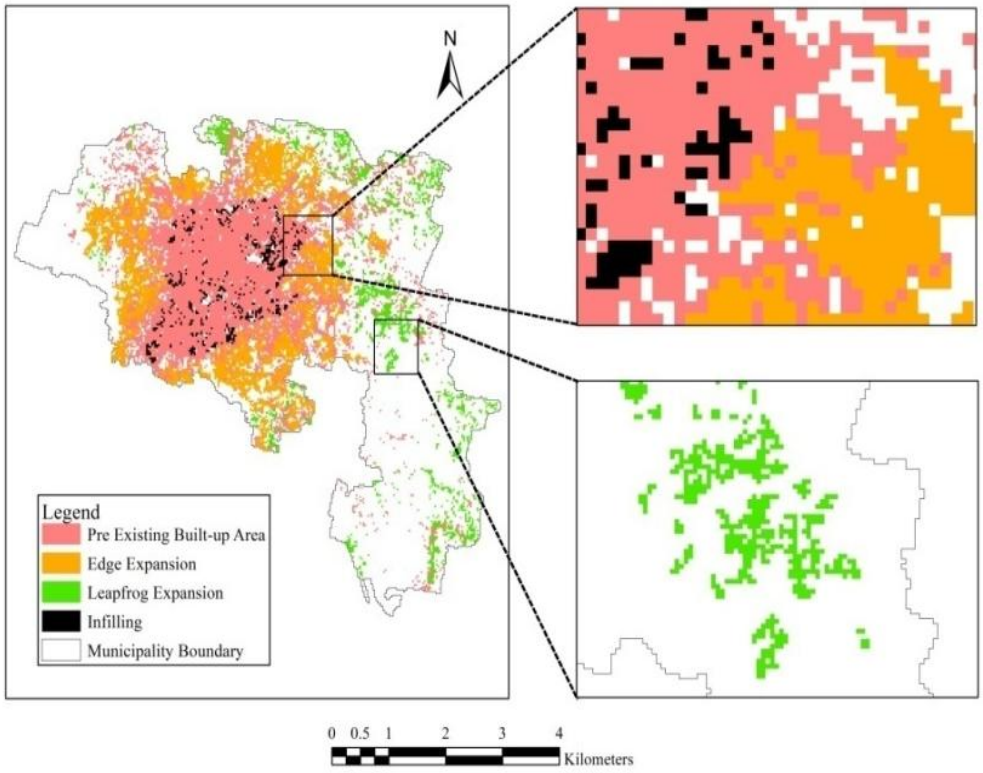

Fig. 2. Typology of urban growth

The digital number (DN) of bands 3, 4 and 6 were converted to space directed radiance or top-of-atmospheric (TOA) radiance (at-sensor spectral radiance) using Equation 2 [53].

$$L\lambda = (LMAX - LMIN) / (QCALMAX - QCALMIN) * (DN - QCALMIN) + LMIN \quad (2)$$

Where L_λ is Spectral radiance in W/ (m^2. steradian.μm), $QCAL_{max}$ is the maximum Quantised calibrated pixel value when DN= 255, $QCAL_{min}$ is the minimum Quantised calibrated pixel value when DN= 1, L_{max} is Spectral radiance that is scaled to $QCAL_{max}$ in W/ (m^2. steradian.μm), L_{min} is Spectral radiance that is scaled to $QCAL_{min}$ in W/ (m^2. steradian.μm).

Equation 3 is used to convert the spectral radiance to the surface- escaping radiance [54]:

$$LT = [(L\lambda - Lu - \tau(1-\varepsilon) Ld]/\tau\varepsilon \quad (3)$$

Where L_T is the blackbody radiance, L_λ is spectral radiance at the sensor's aperture in W/ (m^2. steradian.μm), L_u and L_d are the radiation brightness upward and downward from the atmosphere, respectively. The value of L_u and L_d are 1.68 and 1.77 in W/ (m^2. steradian.μm), respectively. τ is the atmospheric transmission, estimated as 0.77, ε is surface emissivity specified for the target types. Equation 4 is used to compute ε [55]:

$$\varepsilon = \varepsilon_{veg} Pv + \varepsilon_{soil} (1 - Pv) \quad (4)$$

Where ε_{soil} and ε_{veg} are the emissivity of soil and vegetation, respectively. The values of ε_{soil} and ε_{veg} are, estimated as 0.97 and 0.99, respectively. P_v is the proportion of vegetative cover, calculated using Equation 5:

$$Pv = [(NDVI - NDVI_{min})/(NDVI_{max} - NDVI_{min})^2 \quad (5)$$

Where Normalised Difference Vegetation Index (NDVI) can be calculated for the TM sensor by Equation 6 [56].

$$NDVI = (\rho NIR - \rho RED) / (\rho NIR + \rho RED) \quad (6)$$

Where NIR is the near Infrared Band, RED is the red band, and ρ is band reflectivity, and this can be calculated as [53],

$$\rho P = [(\pi * L_\lambda * d2)/(ESUN_\lambda * \cos\theta s)] \quad (7)$$

Where ρP is unit less planetary reflectance, $ESUN_\lambda$ is solar exo-atmospheric irradiances, θ_s is solar zenith angle in degrees, D is the earth-sun distance in astronomical units(au), where 93,000,000=1au [24].

Brightness temperature or radiant temperature (T_B) was calculated from the surface- escaping radiance using Equation 8 [54].

$$T_B = K_2 / \ln[(K_1 / LT) + 1] \quad (8)$$

Where K_1 is the pre-launch calibration constant 1 and 2 in W/ (m^2. steradian.μm). K_1 = 607.76, K_2 = 1260.56.

The brightness or radiant temperature (T_B) of each pixel has been transformed into the kinetic temperature or surface temperature (Ts) using Equation 9.

$$Ts = T_B * \varepsilon^{-(1/4)} \quad (9)$$

$$Ts' = Ts - 273 \quad (10)$$

Where ε is the emissivity (i.e. 0.97). The estimated Ts (in degree Kelvin) was converted into Ts' (surface temperature in degree Celsius) using Equation 10.

3.4.2 Calculation of Land Surface Temperature (LST) from landsat 8/TIRS Data

LST was calculated by applying a structured mathematical algorithm viz., Split-Window (SW) algorithm. It uses the brightness temperature of two bands of TIR, mean and difference in land surface emissivity for estimating LST of an area. The algorithm is as follows:

$$LST = T_B10 + C_1(T_B10 - T_B11) + C_2(T_B10 - T_B11)^2 + C_0 + (C_3 + C_4W)(1-\varepsilon) + (C_5 + C_6W)\Delta\varepsilon \quad (11)$$

Where, C_0 to C_6 is the Split-Window Coefficient values provided in Table 2 [57,58], T_B10 and T_B11 are brightness temperature of band 10 and band 11. ε is the Mean Land Surface Emissivity (LSE) of TIR bands, W is atmospheric water vapour content, and Δε is Difference in LSE.

To obtain the T_B of an area the Top of Atmosphere (TOA) spectral radiance of (L_λ) was required. Equation 12 was adapted to calculate T_B for both the TIR bands.

$$T_B = K_2 / \ln[(K_1 / L_\lambda) + 1] \quad (12)$$

Where K_1 and K_2 are thermal conversion constant and it is different for both TIR bands. For band 10 and 11 value of K_1 is 774.89 and 480.89 respectively and for band 10 and 11 value of K_2 was 1321.08 and 1201.14 respectively, and L_λ was the Top of Atmospheric spectral radiance in W/(m^2 .steradian.μm). Multiplicative rescaling factor of TIR bands was multiplied with the corresponding TIR band, and the additive rescaling facto was added to it for estimating the value of the TOA spectral radiance (Lλ)

$$L_\lambda = ML * Qcal + AL \quad (13)$$

Where ML is the band specific multiplicative rescaling factor. Q_{cal} is the band 10/11 image, and AL is the Band-specific additive rescaling factor. To find LST it is necessary to calculate the land surface emissivity (LSE) of the region. LSE was estimated using Equation 4. The emissivity of vegetation (ε_{veg}) for band 10 and 11 were 0.987 and 0.989 respectively, and the emissivity of soil (ε_{soil}) for band 10 and 11 were 0.971 and 0.977 respectively.

3.5 Identification of Thermal Hotspots and Cool Spots

To distinguish the thermal regions, the LST has been standardised. LST standardisation also gives a better interpretation of LST distribution in the city [24]. Standard scores of the land surface temperatures (LST) were calculated by

Table 2. Split window coefficient value

Constants	C_0	C_1	C_2	C_3	C_4	C_5	C_6
Values	-0.268	1.378	0.183	54.300	-2.238	-129.20	16.400

subtracting the zonal mean LST value, for the whole LST sample (LSTμ), from LST value of every single pixel (LSTx), in each of the LST datasets, and dividing by the sample's standard deviation (LSTσ) as follows:

$$LST = \frac{LSTx - LST\mu}{LST\sigma} \quad (14)$$

The warmer and cooler regions were divided according to the strength of the thermal stability into three categories (spots), defined by the number of standard deviations from the mean (Table 3) [55]. For this study, the undivided warmer area with LST values always higher than the mean LST for Barasat, is designated as 'hotspots' and the entire cooler region, with LST values always lower than the mean LST, is designated as 'cool spots'.

3.6 GIS-based Sectoral-buffer Analysis on Spatiotemporal Dynamics

To analyse the sectoral areal dynamics of the urban growth, and the thermal effect, GIS-based buffer analysis was adopted to encircle the part of the city surrounding the city centre. This buffer system was then divided into eight sectors of equal 45º interval from the north in clockwise direction. The percentage of hot spots, cool spots and the different urban growth modes in the eight sectors were calculated for each time period by using Equation 15.

$$\frac{Area\ related\ to\ a\ specific\ feature\ in\ each\ sector}{Total\ area\ of\ the\ sector}\ X\ 100 \quad (15)$$

Therefore, different urban growth modes, hot spots, and cool spots can be used instead of a specific feature.

3.7 Quantification of the Relative Importance of Different Urban Growth Modes on Controlling the Changing Pattern of LST

Partial Least Squares Regression (PLSR) is a statistical method used to find a relationship between the dependent and explanatory variables. The PLSR method combines the features of multiple linear regression and principal component analysis [59]. The method determines the latent components of the explanatory variables, and that latent components of the dependent variables can explain the majority of the variance. Drawing new relationships among the dependent and explanatory variables is best accomplished by PLSR.

In this study, PLSR is used to quantify the relative importance of the different types of urban growth on the changing nature of LST in the eight 45º sectors. The explanatory variables were the three identified types of growth modes (i.e. infilling, edge expansion and leapfrog). The dependent variable was the change in LST. The entire study area was divided into 150 × 150m grids. Grids, where the urban growth covers at least 20% of the area, were selected for this study.

The spatial statistics for the temporal change in LST and urban growth modes for 1989-2001, 2001-2014 and 2014-2017 were calculated for the selected grids. The grids were then overlaid with the eight 45º sectors to obtain the sector- wise result.

The relationship between the dependent variable (in the present study, changes in the LST) and the explanatory variables (three urban growth modes) are inferred by running PLS regressions

Table 3. Categories of thermal regions and strength of thermal stability

Thermal region	Category of thermal stability	Thermal spot name
hotspots	>2 SD	very hot spot
	1 SD- 2 SD	hot spot
	0-1 SD	warm spot
cool spots	-1–0 SD	cool spot
	-1 SD – (-2 SD)	cold spot
	<-2 SD	very cold spot

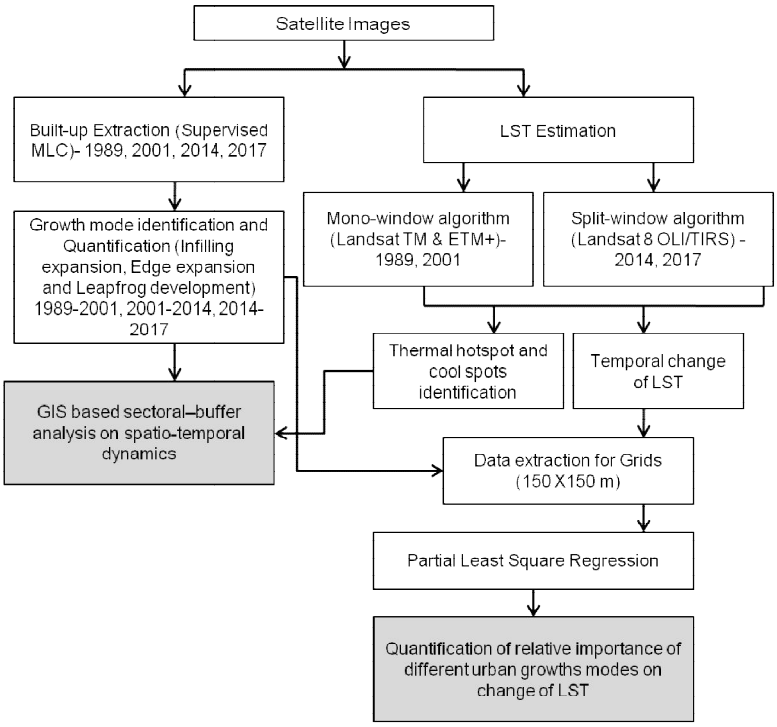

Fig. 3. Flowchart of the methodology

through the XLSTAT-PLS 2008 software. From XLSTAT-PLS, it is possible to explain which sprawl type most strongly interacts with LST changes through the given Variable Importance for the Projection (VIP). The independent variables having large VIP values are the most relevant in explaining the dependent variable.

The flow chart below shows the steps that have been followed in this work.

4. RESULTS AND DISCUSSION

4.1 Accuracy Assessment of Built-up Class

A classification is considered to be correct if it portrays the land cover of the region of concern in an unbiased way. Therefore, an accuracy assessment indicates the degree of confirmation of truth to which the derived image classification agrees [60]. Furthermore, 50 samples were randomly selected from both categories to check the accuracy of the classified maps. The classified images were compared with the Google Earth maps of the respective time periods (1989, 2001, 2014 and 2017). The urban land-use map of Barasat (scale 1:16000) of 2004, prepared by the National Atlas and Thematic Map Organisation (NATMO) was used for this purpose. From the error matrix, the producer's accuracy, user's accuracy and overall accuracy were generated (

Table 4), which met the recommended value [60].

4.2 Directional Pattern of Urban Growth

Over the study period (1989-2017), the urban growth of Barasat has displayed an increasing trend. The data extracted from the satellite images of 1989, 2001, 2014 and 2017 indicated that the urban built-up has expanded from 4.94 sq km in 1989 to 18.87 sq km in 2017. The area under dense built-up in the year 1989 was restricted to a narrow spatial limit (Fig.) Within 28 years, the urban built-up area has substantially increased and nearly engulfed 54% area of the municipality. Apart from being the district head quarter, the high population growth rate expansion may also be attributed to the opening of Adamas University, Brainware University etc. from 2004 that are employing thousands of workers. The urban area has

increased exponentially in Barasat (Fig. 5). The study charted the urban expansion in different directions to understand the locations of the growth of hot zones. Eight major directions (North, North-East, East, South-East, South, South-West, West and North-West) around the city have been used to define the directional areal dynamics of urban expansion for each year. The results are illustrated in Fig. 6.

In 1989, overall growth activity took place in the NW direction (0.96 sq km) followed by the SW direction (0.81 sq km). This is due to the presence and affinity of Barrackpore and Madhyamgram urban agglomeration respectively. The town has expanded minimally in Eastern region (0.37 sq km).

In 2001, the largest growth was observed in the NW (1.57 sq km) direction. The SE and SW directions experienced the second largest growth (1.31 sq km and 1.30 sq km respectively). The S direction had the smallest growth (0.74 sq km).

In 2014, the SE direction has experienced the maximum expansion concentration. In 2014, the SE continued to dominate, with the highest expansion concentration of 2.28 sq km, followed by the NW (2.24 sq km) direction.

In the year 2017, the town expanded mostly in the SE and Eastern directions. The concentration of built-up was least in the SW region in this period (1.76 sq km). Comparatively newer expansions taking place in the SE and Eastern direction may be due to the availability of cheap land for development.

Table 4. Accuracy level of built-up class of classified images for different years

Years	Producer's accuracy	User's accuracy	Overall accuracy
1989	99.34	99.38	98.82
2001	99.72	99.57	98.65
2014	96.26	98.34	95.22
2017	96.30	92.86	85.19

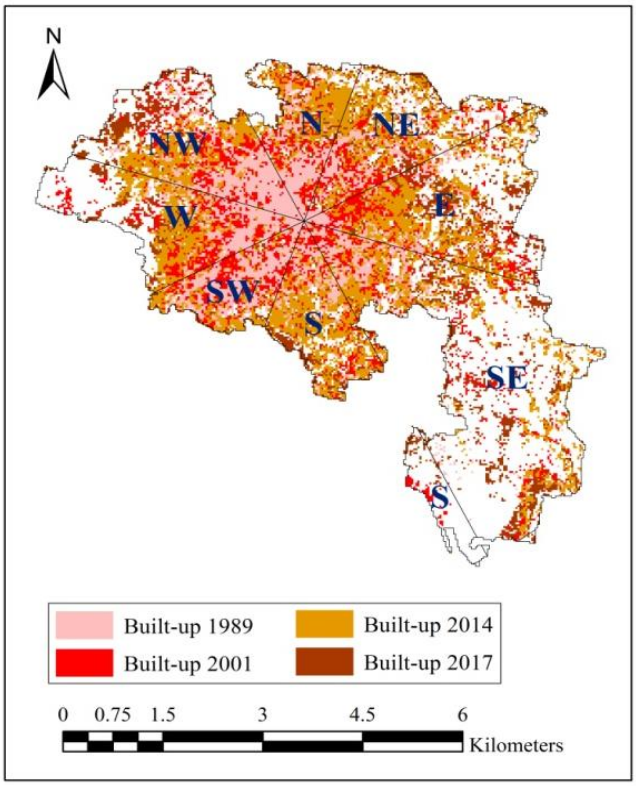

Fig. 4. Urban expansion from 1989 to 2017

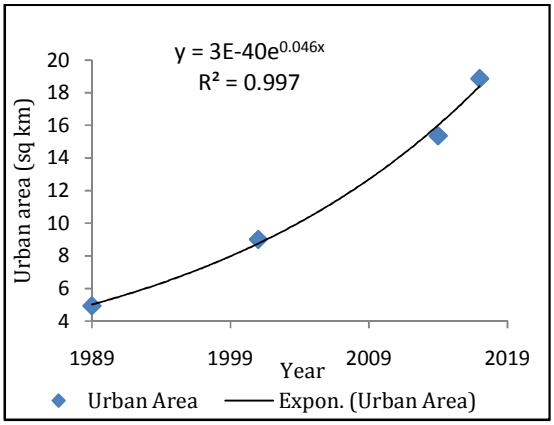

Fig. 5. Growth rate of built-up

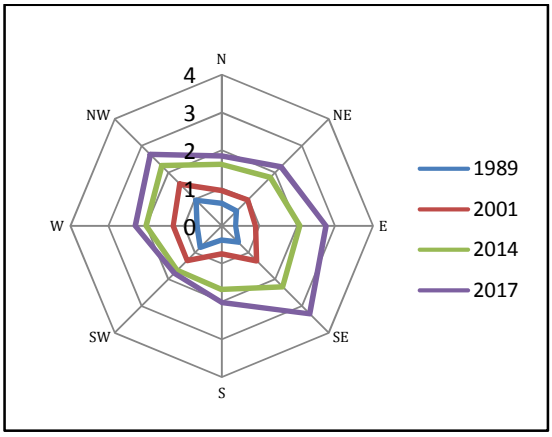

Fig. 6. Directional areal dynamics of built-up

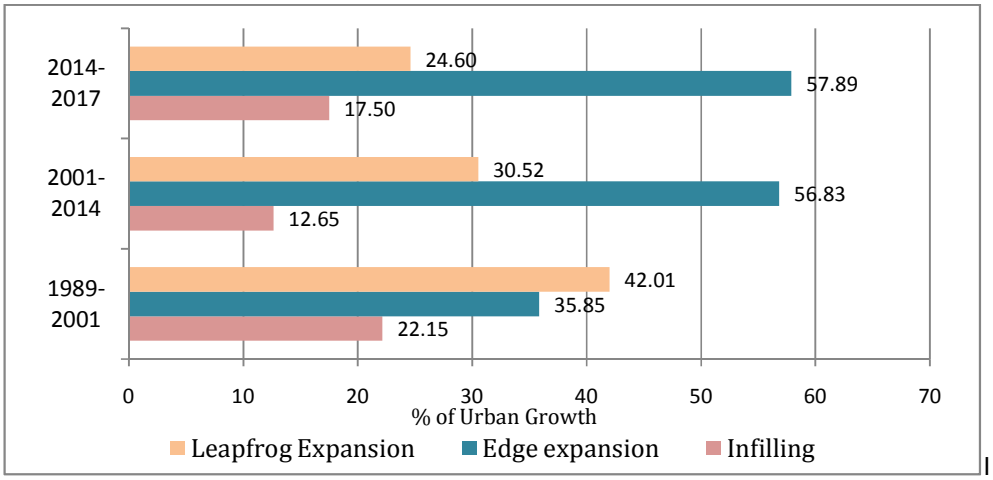

Fig. 7. Changes in the percentage of the three types of urban growth modes

4.3 Identification of Types of Urban Growth

The city has witnessed three major types of urban expansion (i.e., infilling, edge expansion and leapfrog expansion). During 1989 – 2001, the rate of infilling of the vacant areas is lower than the rate of the addition of adjoining patches. The most predominant feature is the leapfrog expansion in this period. During 2001 – 2014, edge expansion was substantially high, which means the urban land was mostly expanded outward from the existing urban centre. Approximately 57% of all new development took place along the established urban patches, 30.52% was leapfrog expansion, and 12.65% was infilling.

Likewise, the edge expansion was found as the dominant mode of expansion, accounting for 58% of the total growth in 2014-2017. Infilling showed an increasing trend, but leapfrog expansion decreased (Fig. 7). This demonstrates that the trend of urban development leaned towards adding plots at the edge of, or adjacent, to the established urban area, which reduces fragmentation and increases compactness.

Leapfrog expansion has contributed significantly to the urban expansion in Barasat. Because of the enormous availability of land, leapfrog expansion was initially highest. Medium leapfrog expansion in later periods, occurred mostly in the eastern part of the city, through the provision of vacant land, low- cost residential housing complexes, and love for nature (Fig. 8). Edge expansion was the primary growth type in the study area in later periods. Overall, the trend is towards the

reduction of fragmentation of urban land and the increase of compaction.

4.4 Analysing the Trend of Land Surface Temperature

In this study, the LSTs of 1989, 2001, 2014 and 2017 for the summer session (April) were derived from Landsat data (Fig. 9). The statistics of LST for 1989–2017 is presented in Table 5. In 1989, the highest LST was 21.69°C, and the lowest LST was 17.92°C in April, while the highest LST found in 2017 was 36.44°C and the minimum was 27.54°C. There has been a constant increase of mean LST from 1989 to 2017 during the summer season. The highest temperature estimated in 1989 (21.69°C) was much lower than the minimum temperature noted in 2017 (27.54°C). The gradual increase in the standard deviation of LST indicates that the variability of LST is also increasing from 1989 to 2017 (Table 5).

4.5 Identification of Hotspots and Cool Spots

The standard score maps provide a powerful visual explanation of hotspots and cool spots (Fig. 10). As discussed in the methodology section, the very hot spots, hot spots, and warm spots are together considered as hotspots, while cool spots, cold spots, and very cold spots are collectively termed cool spots. The compact and continuous urban area contains the warmest zone, called hotspots, with mean standardised LST always greater than the zonal mean. Interestingly the LST values of the discontinuous, scattered urban zones, with non- built-up activities, are always lower than the zonal mean LST in Barasat.

This strong heating in the compact urban area is caused mostly by the high heat capacity of artificial surfaces such as asphalt, concrete, and roofing materials. With continuous urban

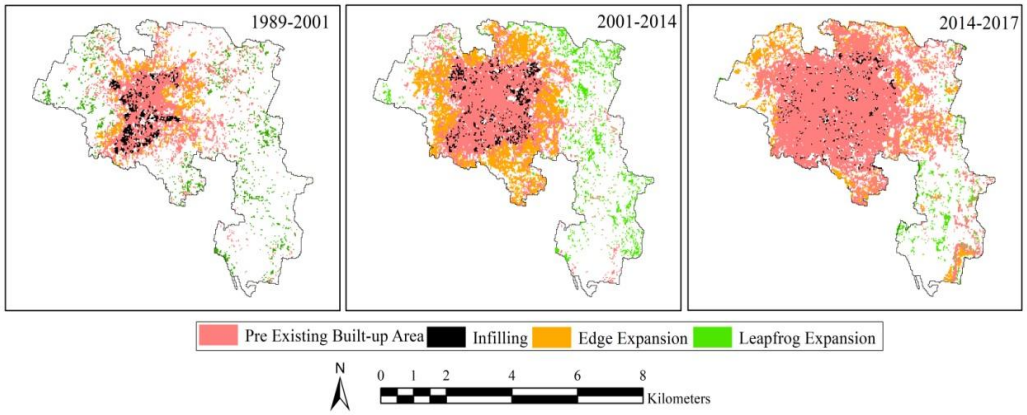

Fig. 7. Different urban growth modes of Barasat

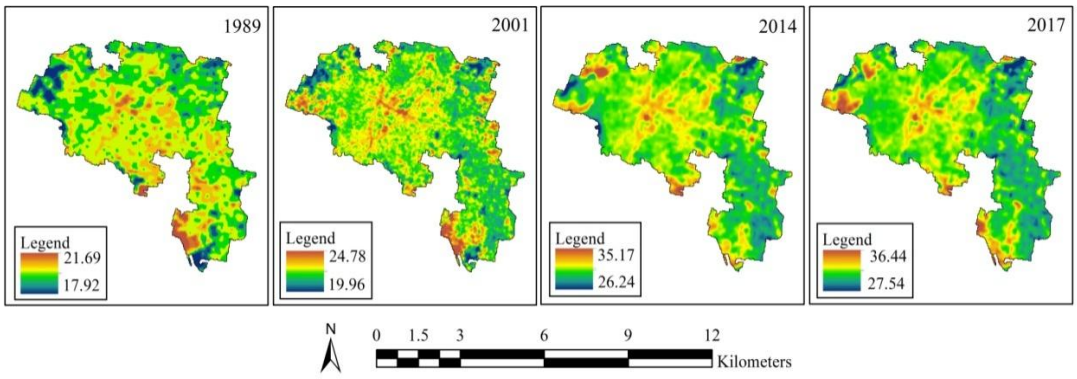

Fig. 8. LST (°C) of four selected years

expansion and heat accumulation in the established city centre, the thermal contrast between the core city and the surroundings has increased markedly from 0.27 to 1.40°C from 1989 to 2017 (Table 6). This intra-urban temperature difference provides a good indication of how different urban pattern corresponds to the thermal environment.

4.6 Sectoral Distribution of Urban Growth Modes and Thermal Effects

4.6.1 Sectoral distribution of urban growth modes

The percentage share of urban growth modes in the eight sectors was calculated for each time period (1989-2001, 2001-2014 and 2014-2017) using Equation 15. To distinguish the level of concentration of urban growth in eight sectors, the percentage share is categorised into three classes (i.e., “high”, “medium” and “low”) using standard deviation (Fig. 11).

The map (Fig. 11) indicates that during the period from 1989-2001, the NW, W and SW sectors experienced maximum infilling, the NW, W , SW, N, NE sectors have mostly experienced edge expansion, and the S sector experienced leapfrogging.

The urban land that was developed through the edge and leapfrog expansion in 1989-2001 eventually become connected, and more compact, through the infilling in the period of 2001 – 2014. Excluding the N and NE, all the sectors experienced medium to high infilling, and excluding the SE, all sectors experienced medium to high edge expansion in 2001- 2014.

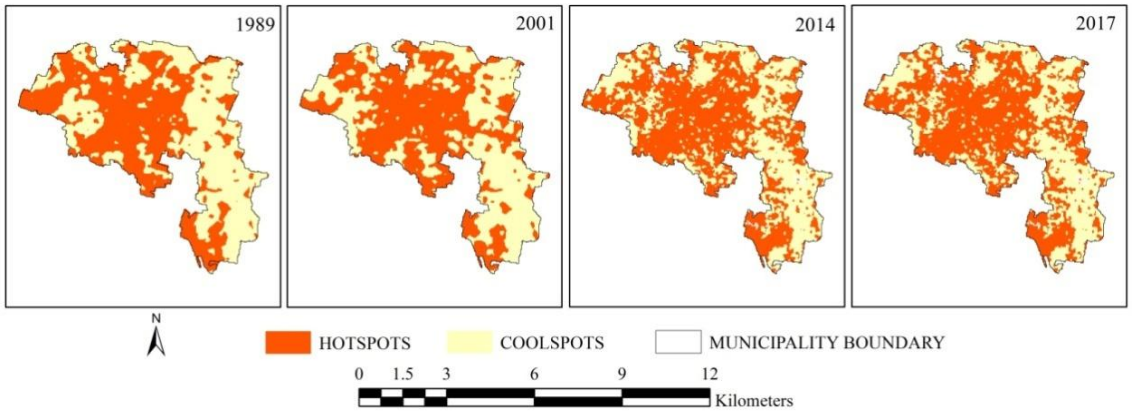

Fig. 9. Standardised land surface temperature pattern in the Barasat municipality

Table 5. LST statistics

Year	Highest temperature (°C)	Lowest temperature (°C)	Mean temperature (°C)	Standard deviation
1989	21.69	17.92	19.27	0.36
2001	24.78	19.96	21.92	0.63
2014	35.17	26.24	29.78	0.97
2017	36.44	27.54	31.10	1.06

Table 6. Differences in mean temperature in hotspots and cool spots

Year	Mean temperature (°C) of hotspots	Mean temperature (°C) of cool spots	Difference of temperature (°C)
1989	19.38	19.11	0.27
2001	22.34	21.35	0.99
2014	30.34	29.13	1.21
2017	31.76	30.36	1.40

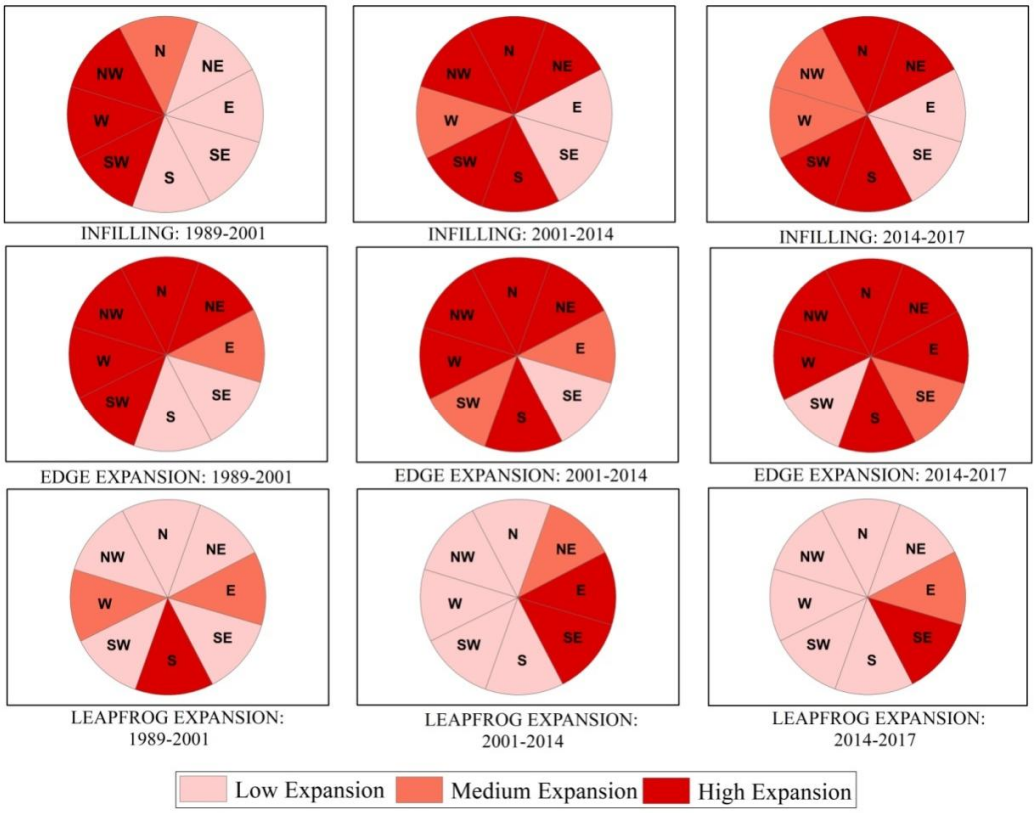

Fig. 10. Sectoral analysis on spatiotemporal dynamics of urban growth modes

In 2014 – 2017, the infilling has remained high in the NE, N, SW, S sectors. The edge expansion was high only in the S, W, NW, N, NE and E sectors. Leapfrogging was high in the SE, and medium in the E sector.

Leapfrog expansion was random in 1989-2001, because of the ample availability of land. Leapfrog expansion was restricted in 2001-2014 and 2014-2017 in the western part of the city (SW, W & NW sectors), and the N and S sectors because of the unavailability of vacant land for development. The continuous decrease of edge expansion in the SW is prominent, while the sector has experienced maximum possible urban growth. In general, the western part and the N and S sectors of the city have experienced maximum infilling and edge expansion, and the eastern part of the city (NE, E, SE sectors), is characterised by the highest leapfrog expansion.

4.6.2 Sectoral distribution of thermal effects-

The sector- wise thermal effects (hotspots and cool spots) in 1989, 2001, 2014 and 2017 are depicted in Fig. 12. The concentration of the thermal effect in the eight sectors has been categorised into three classes “high”, “medium” and “low” using Equation 15.

The highest concentration of hotspots is found in the western part of the study area in 1989, in the western part and the S sectors in 2001, in the western part and S and N sectors in 2014, and in the western part, S, N and NE sectors in 2017.

It can be stated that initially the high concentration of hotspots was in the western part of the study area, which gradually over the years spread towards the eastern part of the site, expanding over the N and S sectors. The high concentration of cool spots has been observed in the E and SE sectors in 1989, 2001 and 2014, and only in the SE in 2017. The spatiotemporal dynamics of thermal effects portrays the gradual spreading of the concentration of hotspots and shrinking concentration of cool spots.

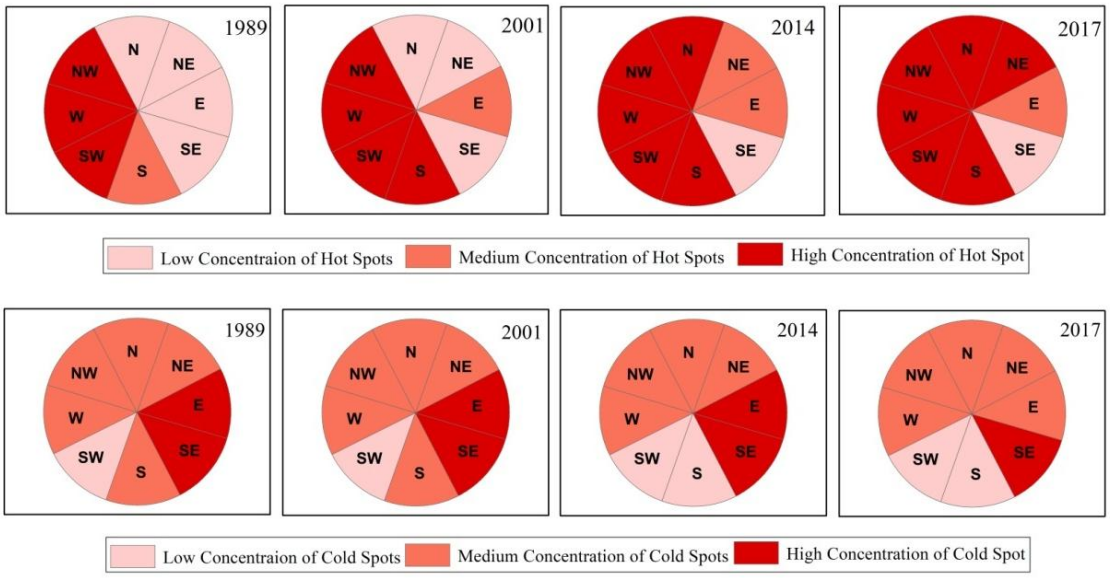

Fig. 11. Spatial patterns of (a) hotspot and (b) cool spot in eight sectors

4.6.2 Comparing the sectoral distribution of urban growth modes and thermal effects

The sectoral distribution of urban growth modes and thermal effects share certain common characteristics. For example, leapfrog expansion is most common in the eastern part, while the western portion of the site is characterised by infilling and edge expansion. The western part also experienced higher concentrations of hotspots compared to the other sectors. The high concentrations of cool spots are found in the S and SE sectors.

This implies that the high hotspot concentrations are already in the developed urban land. The eastern part of the city covered the key areas of cool spots, which correspond to new urban development. This indicates that hotspot is sensitive to infilling and edge expansion, where cool spots are responsive to leapfrog expansion.

4.7 Relative Importance Urban Growth Modes on Controlling Changing Pattern of LST

The relative importance of the different urban growth modes in the change of LST was revealed using Partial Least Squares Regression (PLSR), and the Variable Importance in the Projection (VIP), which are the measures of the importance of explanatory variables on the dependent variable. VIP score is provided in Table 7. If the VIP score is greater than the suggested threshold of 0.8, the variables are considered to contribute significantly [61]. This threshold allows identification of important variables.

As expected, higher VIP values are found for edge expansion for all eight sectors (VIP > 0.8), except for the NE sector. This implies that edge expansion is identified as the strongest factor affecting the changes of LST. Infilling development is an important contributing factor in the SW, W and N sectors, while leapfrog expansion is found to be significant in the S, SE and NE sectors.

The increase in impervious surface area, by the addition of adjoining urban patches along the edge of the older patch, makes the older patch larger. Edge expansion is identified as the most significant factor affecting the change in LST. The overall low VIP values (≤0.8) in most of the sectors for infilling and leapfrog expansion, indicate their relatively low importance affecting the LST change.

The PLSR methodology is beneficial and novel in this context because by using this elimination of codependency among the variables is possible. It encourages an unbiased view of the contribution of the different types of urban growth in the change in LST.

Table 7. Variable importance in the projection (VIP)

Variable	Sectors							
	SW	S	SE	W	E	NW	NE	N
Infilling	**1.15**	0.63	0.36	**0.93**	0.61	0.29	0.58	**1.04**
Edge expansion	**1.21**	**1.39**	**1.32**	**1.38**	**1.41**	**1.60**	0.21	**1.28**
Leapfrog expansion	0.46	**0.82**	**1.06**	0.49	0.79	0.59	**1.61**	0.52

5. CONCLUSION

An overview of urban growth, the thermal environment, and their relationship has been explored in the Barasat municipality.

The spatiotemporal growth of urban built-up has been calculated for each different types of urban growth which has been identified and quantified. The directional areal dynamics of built-up illustrates how and why the direction of urban expansion changes with time. The estimated LST and standard score identify the SUHI and SUHS as thermal hotspots and cool spots respectively. The GIS-based sectoral-buffer analysis of the spatiotemporal dynamics has been used to demonstrate how the different sectors of a city experience different types of urban growth, hotspot, and cool spot effects. This methodology indicates that hotspots are sensitive to infilling and edge expansion, while cool spots correspond to leapfrog expansion. PLSR between the growth modes and change in LST reveals that edge expansion is the most important factor in determining LST change.

The spatially compact, connected, homogeneous urban structures of the older areas help maintain warmer urban temperatures, as opposed to the new scatted developments. This difference is mainly due to surface configuration and complexity. The nature of the temperature of any surface depends on the thermal inertia for that particular surface. Thermal inertia is dependent on the composition of the surface. Due to their higher thermal capacity, the thermal inertia for the compact, old urban area leads to higher temperatures than those of new, fragmented urban developments.

One good thing about the proposed methodology is that it can be easily computed and used in any urban area. This research enhances the scientific knowledge on urban growth types and the thermal environment interact. More edge expansion will significantly increase LST, exacerbating the SUHI or hotspot phenomena. Thus the impact of urban expansion on LST can be mitigated by optimising its spatial configuration. The lack of understanding of the heating and cooling effect from urban growth limits urban design and planning. Future planning should be geared towards strategically mitigating the rising trend of temperature faced by the residents. The results of this study are significant in both environmental management and urban planning.

COMPETING INTERESTS

Authors have declared that no competing interests exist.

REFERENCES

1. Taubenböck H, Wegmann M, Berger C, Breunig M, Roth A, Mehl H. Spatiotemporal analysis of Indian megacities. Proceedings of the International Archives of the Photogrammetry, Remote Sensing and Spatial Information Sciences (ISPRS). 2008;37:75-82.
2. Available:www.un.org/En/Development/Desa/Population/.../Urbanization/Wup2011_Report.Pdf
3. Census of India. Final population totals; 2011a.
   Available:http://censusindia.gov.in/2011census/censusinfodashboard/index.html
   (Accessed August 23, 2018)
4. JNNURM (Jawaharlal Nehru National Urban Renewal Mission). High powered expert committee report, JNNURM; 2011.
   Available:http://jnnurm.nic.in/wp-content/uploads/2011/10/HPEC-Sept.-27-OVC.pdf
   (Accessed August 23, 2018)
5. Inostroza L, Baur R, Csaplovics E. Urban sprawl and fragmentation in Latin America: A dynamic quantification and characterization of spatial patterns. J Environ Manage. 2013;115:87-97.
   DOI: 10.1016/j.jenvman.2012.11.007
6. Berling-Wolff S, Wu J. Modeling urban landscape dynamics: A case study in

Phoenix, USA. Urban Ecosyst. 2004;7(3): 215-240.
DOI: 10.1023/b:ueco.0000044037.23965.45

7. Xu C, Liu M, Zhang C, An S, Yu W, Chen J. The spatiotemporal dynamics of rapid urban growth in the Nanjing metropolitan region of China. Landsc Ecol. 2007;22(6): 925-937.
DOI: 10.1007/s10980-007-9079-5
8. Liu Z, He C, Zhang Q, Huang Q, Yang Y. Extracting the dynamics of urban expansion in China using DMSP-OLS nighttime light data from 1992 to 2008. Landsc Urban Plan. 2012;106(1):62-72.
DOI: 10.1016/j.landurbplan.2012.02.013
9. Ghani N, Abidin S. A modified landscape expansion index algorithm for urban growth classification using satellite remote sensing image. Advanced Science Letters. 2018;24(3):1843-1846.
DOI: 10.1166/Asl.2018.11173
10. Liu X, Li X, Chen Y, Tan Z, Li S, Ai B. A new landscape index for quantifying urban expansion using multi-temporal remotely sensed data. Landsc Ecol. 2010;25(5):671-682.
DOI: 10.1007/S10980-010-9454-5
11. Voogt J, Oke T. Thermal remote sensing of urban climates. Remote Sens Environ. 2003;86(3):370-384.
DOI: 10.1016/s0034-4257(03)00079-8
12. Balchin W, Pye N. A micro-climatological investigation of bath and the surrounding district. Quarterly Journal of the Royal Meteorological Society. 1947;73(317-318): 297-323.
DOI: 10.1002/qj.49707331706
13. Comarazamy D, González J, Luvall J, Rickman D, Mulero P. A land–atmospheric interaction study in the coastal tropical city of San Juan, Puerto Rico. Earth Interact. 2010;14(16):1-24.
DOI: 10.1175/2010ei309.1
14. Shan B, Li X, Pan T et al. Effect of shaddock albedo addition on the properties of frankfurters. J Food Sci Technol. 2014; 52(7):4572-4578.
DOI: 10.1007/s13197-014-1467-7
15. Oke T. The energetic basis of the urban heat island. Quarterly Journal of the Royal Meteorological Society. 1982;108(455):1-24.
DOI: 10.1002/qj.49710845502
16. Yow D. Urban heat islands: Observations, impacts, and adaptation. Geography Compass. 2007;1(6):1227-1251.
DOI: 10.1111/j.1749-8198.2007.00063.x
17. Yuan F, Bauer M. Comparison of impervious surface area and normalized difference vegetation index as indicators of surface urban heat island effects in Landsat imagery. Remote Sens Environ. 2007;106(3):375-386.
DOI: 10.1016/j.rse.2006.09.003
18. Roth M, Oke T, Emery W. Satellite-derived urban heat islands from three coastal cities and the utilization of such data in urban climatology. Int J Remote Sens. 1989; 10(11):1699-1720.
DOI: 10.1080/01431168908904002
19. Nassar A, Blackburn G, Whyatt J. Dynamics and controls of urban heat sink and island phenomena in a desert city: Development of a local climate zone scheme using remotely-sensed inputs. International Journal of Applied Earth Observation and Geo information. 2016; 51:76-90.
DOI: 10.1016/j.jag.2016.05.004
20. Yuan F, Wu C, Bauer M. Comparison of spectral analysis techniques for impervious surface estimation using landsat imagery. Photogrammetric Engineering & Remote Sensing. 2008;74(8):1045-1055.
DOI: 10.14358/pers.74.8.1045
21. Sobrino J, Jimenez-Muoz J, Soria G, et al. Land surface emissivity retrieval from different VNIR and TIR sensors. IEEE Transactions on Geoscience and Remote Sensing. 2008;46(2):316-327.
DOI: 10.1109/tgrs.2007.904834
22. Bruns J, Simko V. Stable hotspot analysis for intra-urban heat islands. GI_Forum. 2017;1:79-92.
DOI: 10.1552/giscience2017_01_s79
23. Tran D, Pla F, Latorre-Carmona P, Myint S, Caetano M, Kieu H. Characterizing the relationship between land use land cover change and land surface temperature. ISPRS Journal of Photogrammetry and Remote Sensing. 2017;124:119-132.
DOI: 10.1016/j.isprsjprs.2017.01.001
24. Walawender J, Szymanowski M, Hajto M, Bokwa A. Land surface temperature patterns in the urban agglomeration of krakow (Poland) derived from landsat-7/ETM+ data. Pure and Applied Geophysics. 2013;171(6):913-940.
DOI: 10.1007/s00024-013-0685-7
25. Qiao Z, Tian G, Zhang L, Xu X. Influences of urban expansion on urban heat island in beijing during 1989–2010. Advances in Meteorology. 2014;1-11.

DOI: 10.1155/2014/187169
26. Li J, Song C, Cao L, Zhu F, Meng X, Wu J. Impacts of landscape structure on surface urban heat islands: A case study of Shanghai, China. Remote Sens Environ. 2011;115(12):3249-3263.
DOI: 10.1016/j.rse.2011.07.008
27. Wang Y, Hu B, Myint S, Feng C, Chow W, Passy P. Patterns of land change and their potential impacts on land surface temperature change in Yangon, Myanmar. Science of the Total Environment. 2018;643:738-750.
DOI: 10.1016/j.scitotenv.2018.06.209
28. Kłysik K, Fortuniak K. Temporal and spatial characteristics of the urban heat island of Łódź, Poland. Atmos Environ. 1999; 33(24-25):3885-3895.
DOI: 10.1016/s1352-2310(99)00131-4
29. Saaroni H, Ben-Dor E, Bitan A, Potchter O. Spatial distribution and microscale characteristics of the urban heat island in Tel-Aviv, Israel. Landsc Urban Plan. 2000; 48(1-2):1-18.
DOI: 10.1016/s0169-2046(99)00075-4
30. Unwin D. The synoptic climatology of birmingham's urban heat island, 1965-74. Weather. 1980;35(2):43-50.
DOI: 10.1002/j.1477-8696.1980.tb03484.x
31. Adebayo Y. Land-use approach to the spatial analysis of the urban 'heat island' in Ibadan, Nigeria. Weather. 1987;42(9):273-280.
DOI: 10.1002/j.1477-8696.1987.tb04906.x
32. Graham E. The urban heat island of Dublin city during the summer months. Irish Geography. 1993;26(1):45-57.
DOI: 10.1080/00750779309478717
33. Lee D. Urban warming? - An analysis of recent trends in London's heat island. Weather. 1992;47(2):50-56.
DOI: 10.1002/J.1477-8696.1992.Tb05773.X
34. Parker D. Urban heat island effects on estimates of observed climate change. Wiley Interdisciplinary Reviews: Climate Change. 2009;1(1):123-133.
DOI: 10.1002/wcc.21
35. Streutker D. A remote sensing study of the urban heat island of Houston, Texas. Int J Remote Sens. 2002;23(13):2595-2608.
DOI: 10.1080/01431160110115023
36. Roth M, Chow W. A historical review and assessment of urban heat island research in Singapore. Singap J Trop Geogr. 2012; 33(3):381-397.
DOI: 10.1111/sjtg.12003
37. Zhao J, Dai D, Lin T, Tang L. Rapid urbanisation, ecological effects and sustainable city construction in Xiamen. International Journal of Sustainable Development & World Ecology. 2010; 17(4):271-272.
DOI: 10.1080/13504509.2010.493318
38. Zhang D, Shou Y, Dickerson R. Upstream urbanization exacerbates urban heat island effects. Geophys Res Lett. 2009;36(24).
DOI: 10.1029/2009gl041082
39. Sung C. Mitigating surface urban heat island by a tree protection policy: A case study of The Woodland, Texas, USA. Urban For Urban Green. 2013;12(4):474-480.
DOI: 10.1016/j.ufug.2013.05.009
40. Moss J, Doick K, Smith S, Shahrestani M. Influence of evaporative cooling by urban forests on cooling demand in cities. Urban For Urban Green; 2018.
DOI: 10.1016/j.ufug.2018.07.023
41. Wilkinson S, Reed R. Green roof retrofit potential in the central business district. Property Management. 2009;27(5):284-301.
DOI: 10.1108/02637470910998456
42. Synnefa A, Santamouris M, Akbari H. Estimating the effect of using cool coatings on energy loads and thermal comfort in residential buildings in various climatic conditions. Energy Build. 2007;39(11): 1167-1174.
DOI: 10.1016/j.enbuild.2007.01.004
43. Qiao Z, Tian G, Zhang L, Xu X. Influences of urban expansion on urban heat island in beijing during 1989–2010. Advances in Meteorology. 2014;2014:1-11.
DOI: 10.1155/2014/187169
44. Li X, Zhang L, Liang C. A GIS-based buffer gradient analysis on spatiotemporal dynamics of urban expansion in Shanghai and its major satellite cities. Procedia Environ Sci. 2010;2:1139-1156.
DOI: 10.1016/j.proenv.2010.10.123
45. Deng C, Wu C. A spatially adaptive spectral mixture analysis for mapping subpixel urban impervious surface distribution. Remote Sens Environ. 2013; 133:62-70.
DOI: 10.1016/j.rse.2013.02.005
46. Bhatti S, Tripathi N. Built-up area extraction using Landsat 8 OLI imagery. GIsci Remote Sens. 2014;51(4):445-467.
DOI: 10.1080/15481603.2014.939539
47. Bhatta B. Analysis of urban growth pattern using remote sensing and GIS: A case

study of Kolkata, India. Int J Remote Sens. 2009;30(18):4733-4746.
DOI: 10.1080/01431160802651967
48. Sudhira H, Ramachandra T, Jagadish K. Urban sprawl: Metrics, dynamics and modelling using GIS. International Journal of Applied Earth Observation and Geoinformation. 2004;5(1):29-39.
DOI: 10.1016/j.jag.2003.08.002
49. Li X, Yeh A. Analyzing spatial restructuring of land use patterns in a fast growing region using remote sensing and GIS. Landscape and Urban Planning. 2004; 69(4):335-354.
DOI: 10.1016/j.landurbplan.2003.10.033
50. Thapa R, Murayama Y. Urban mapping, accuracy, & image classification: A comparison of multiple approaches in Tsukuba City, Japan. Applied Geography. 2009;29(1):135-144.
DOI: 10.1016/j.apgeog.2008.08.001
51. Liu X, Ma L, Li X, Ai B, Li S, He Z. Simulating urban growth by integrating landscape expansion index (LEI) and cellular automata. International Journal of Geographical Information Science. 2013; 28(1):148-163.
DOI: 10.1080/13658816.2013.831097
52. Mukherjee K, Ray R. An analytical study on the relationship between LULC dynamics and land surface thermal environment-a case study on Barasat municipal area, North 24 Parganas, West Bengal, India. International Journal of Remote Sensing & Geoscience. 2017; 6(2).
53. Sobrino J, Li Z, Stoll M, Becker F. Multi-channel and multi-angle algorithms for estimating sea and land surface temperature with ATSR data. Int J Remote Sens. 1996;17(11):2089-2114.
DOI: 10.1080/01431169608948760
54. Comarazamy D, González J, Luvall J, Rickman D, Mulero P. A land–atmospheric interaction study in the coastal tropical city of San Juan, Puerto Rico. Earth Interact. 2010;14(16):1-24.
DOI: 10.1175/2010ei309.1
55. Stathopoulou M, Synnefa A, Cartalis C, Santamouris M, Karlessi T, Akbari H. A surface heat island study of Athens using high-resolution satellite imagery and measurements of the optical and thermal properties of commonly used building and paving materials. International Journal of Sustainable Energy. 2009;28(1-3):59-76.
DOI: 10.1080/14786450802452753
56. Yu X, Guo X, Wu Z. Land surface temperature retrieval from landsat 8 TIRS—comparison between radiative transfer equation-based method, split window algorithm and single channel method. Remote Sens (Basel). 2014;6(10): 9829-9852.
DOI: 10.3390/rs6109829
57. Yuan F, Bauer M. Comparison of impervious surface area and normalized difference vegetation index as indicators of surface urban heat island effects in Landsat imagery. Remote Sens Environ. 2007;106(3):375-386.
DOI: 10.1016/j.rse.2006.09.003
58. Skoković D, Sobrino JA, Jimenez-Munoz JC, Soria G, Juşien Y, Mattar C, Cristóbal J. Calibration and validation of land surface temperature for landsat8-TIRS sensor. In LPVE (Land Product Validation and Evolution). ESA/ESRIN; 2014.
59. Abdi H. Partial least squares regression and projection on latent structure regression (PLS Regression). Wiley Interdisciplinary Reviews: Computational Statistics. 2010;2(1):97-106.
DOI: 10.1002/wics.51
60. Lucas IF, JM. Frans, VD. Wel. Accuracy assessmentof satellite derived land 2 over data: A review. Photog Ramm Etric Engineering & Rem ote Sensing. 1994; 60(4):410-432.
61. Wold H. Partial least squares. Kotz S, Johnson N (eds.). Encyclopedia of statistical sciences. New York: J. Wiley. 1985;6:581-591.

Peer-review history:
The peer review history for this paper can be accessed here:
http://www.sciencedomain.org/review-history/26489